The 8th International Supercritical CO_2 Power Cycles Symposium
February 27 – 29, 2024, San Antonio, Texas
Paper # 70

Design and Optimization of a 3-Stage Axial Supercritical CO_2 Compressor

Saugat Ghimire
Graduate Research Assistant
GTSL, University of Cincinnati
Cincinnati, Ohio

Matthew Ha
Graduate Research Assistant
GTSL, University of Cincinnati
Cincinnati, Ohio

Justin Holder
Graduate Research Assistant
GTSL, University of Cincinnati
Cincinnati, Ohio

Mark Turner
Professor Emeritus
University of Cincinnati
Cincinnati, Ohio

ABSTRACT

This paper presents the detailed design and optimization of a three-stage axial supercritical carbon dioxide (sCO_2) compressor to support the advancement of sCO_2 power cycles, recognized for their efficiency and compactness in energy conversion. The three-stage design is a scaled model of the original nine-stage 100 MW design. The aerodynamic design and structural analysis were performed at the University of Cincinnati, and the results are presented. The first stage of the design has been meticulously manufactured and experimentally tested at University of Notre Dame Turbomachinery Laboratory. The design process starts with the preliminary design process, considering the required operating boundary conditions and geometrical constraints for full stage design. The design is then scaled down to 3-stage based on the power limitation. The definition for design parameters has been inspired from the EEE HPC design and tweaked to fit the sCO_2 operation. Axisymmetric analysis is performed next and the parametric geometry modeler -Tblade3 has been used to create 3D blade geometry from the results which can then be exported for the 3D CFD analysis and optimization. An efficiency of 89.85% is predicted for the final design at the design point.

INTRODUCTION

The pursuit of high-efficiency, compact, and environmentally sustainable power generation systems has led to a renewed interest in supercritical carbon dioxide (sCO_2) technology as a promising working fluid for various energy conversion applications. Among the critical components in sCO_2 power cycles, the compressor plays a pivotal role in enhancing overall system performance. This paper presents a comprehensive study on the design and optimization of a 3-stage axial compressor tailored for supercritical CO_2 applications.

Supercritical CO_2 technology, owing to its favorable thermophysical properties, offers a compelling alternative to conventional power cycles utilizing steam or organic Rankine fluids. Operating at pressures and temperatures beyond their critical points, sCO_2 systems exhibit higher energy densities, reduced equipment sizes, and improved thermal efficiencies (Brun et al., 2017). These attributes make them particularly attractive for next-generation power plants, waste heat recovery systems, and various industrial processes.

The compressor, as an integral component of sCO_2 power cycles, plays a vital role in compressing the working fluid to the required high pressures. Achieving high efficiency and robust performance in such compressors is a multi-faceted engineering challenge that necessitates a holistic approach, encompassing preliminary design considerations, advanced computational fluid dynamics (CFD) simulations, and subsequent optimization. (Wang et al., 2004) have looked at the application of sCO_2 Brayton cycle for design of axial compressors and have shown that a high efficiency is achievable while operating near supercritical point and leads to a more compact size then helium compressors.

The primary objective of this research is to develop a 3-stage axial compressor tailored to the unique demands of sCO_2 applications. This design is part of the full-scale 9 stage design. The three stage design condition on a P-h diagram is shown below in Figure 1. The design process encompasses critical parameters such as size scaling, blade counts, clearances, rotational speeds, pressure ratios, and overall efficiency. By leveraging state-of-the-art CFD techniques, this study aims to refine the design iteratively, maximizing compressor performance while adhering to practical constraints.

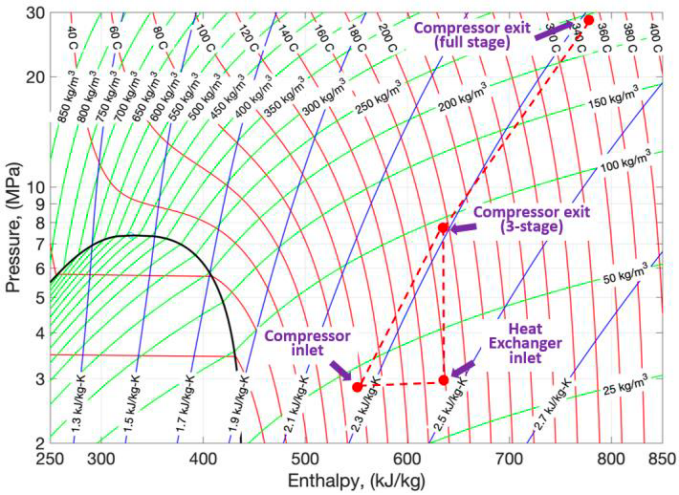

Figure 1 Three stage design condition on a P-h diagram (Kang et al., 2021)

METHODOLOGY

I. PRELIMINARY DESIGN

The full-scale compressor is rated at 100 MW and has nine stages. To facilitate testing, the full-scale design is scaled down to rig design which is a 3-stage, 9 MW rating for which the detailed design is performed. The design coefficients were mostly inspired by GE's EEE design, and a few changes were made to accommodate for the operation with sCO_2 and based on the rig size and power available. The sub-scale compressor is scaled using size and rpm. Furthermore, power limits from the testing facility define maximum rpm for the sub-scale design.

The preliminary design process is performed in an in house non-proprietary axisymmetric turbomachinery system (T-AXI) with built-in loss models that can create new multistage compressors form a table of design parameters. More information on T-AXI can be found in (Turner et al., 2011). The meanline compressor design code TC-DES was modified and rewritten in python to incorporate real gas and sCO_2 application into Py-C-DES, a python-based sCO_2 axial compressor meanline code. The thermodynamic properties of sCO_2 are obtained using REFPROP and is used by Py-C-DES to perform the meanline calculation followed by axisymmetric solve in T-AXI solver to arrive at a suitable preliminary geometry and flow paths. The details of the meanline tool development is presented in (Wells and Turner, 2021)

The approach to design is to build on something that is known and tweak it a bit. The design for this application is inspired from the GE EEE 10 stage machine. The compressor for the sCO_2 project is an advanced technology compressor, 9-stage unit designed to produce the total enthalpy rise of 217 kJ/kg. The compressor rotation speed is set by the test rig motor power and rotor tip speed is determined by the stall margin requirement rather than being a direct design specification.

The blade count for the meanline design was calculated through the solidity values defined for rotors and stators which were inspired from the GE EEE HPC. (Cline et al.; Holloway et al.,). Solidity distributions vary across stages, with higher solidities in front stages where relative Mach numbers are highest. The stator solidities were strategically adjusted based on the expected variability in front stages

and increased aerodynamic loadings in rear stages due to axial velocity diffusion. Another factor that determines the blade counts is the aspect ratio of the rotor and stator blades which were also derived from EEE and were determined mostly based on aeromechanical considerations. The absolute Mach number, inlet flow angle, rotor speed and enthalpy rise through stages were determined based on the calculation of flow coefficient and work coefficient to stay at the islands of highest efficiency per Smith's chart. (David Hall, 2011). Since the details of this design are proprietary, the details of meanline design for a representative case is presented in (Wells and Turner, 2021).

II. THREE STAGE DESIGN

The three-stage baseline design was obtained by scaling the nine-stage axisymmetric design by size and RPM due to the non-perfect gas properties of sCO_2 that results in a non-linear scaling of boundary conditions. Mass flow rate is calculated based on total enthalpy rise through three stages. The square root of the mass flow rate ratio then gave the scaling factor used to calculate the rotational speed equaling 19,800 RPM. The linear dimensions were then scaled for size with this scaling factor. Everything else was then kept identical between the full-scale and the rig design from Mach number standpoint. The Reynolds number could not be matched due to reduced size despite having the same inlet condition. This process defined the requirements for the design. The power of 9 MW and mass-flow of 116.56 kg/s with hub radius of 0.102 m. The clearance-to-tip ratio was retained, and simple axisymmetric adiabatic efficiency was targeted for 92.5%.

III. 3D DESIGN AND OPTMIZATION

i. 3D Geometry and Meshing

After the preliminary design is performed in T-AXI, the initial T-Blade3 geometry file, velocity triangles and boundary conditions are obtained. The input from T-AXI is optimized using an Euler based CFD program, MISES (Drela and Giles, 1987). MISES optimization allows for the local improvement of spanwise quasi-3D flow effects and provides a suitable baseline geometry for 3D RANS analysis and design optimization. The multi-fidelity, off-design, optimization process for turbomachinery design is described in detail by (Ha et al., 2022) for the first stage of the axial sCO_2 compressor. This methodology was then used to design the second and third stages of the three-stage 9 MW design.

From T-AXI, along with the axisymmetric results, files containing the parametric definitions of the 3D blade are also generated which is then used by T-Blade3 (Siddappaji et al., 2012) (Sharma and Turner, 2021), an in-house developed general parametric 3D blade geometry builder to generate all blade rows for the compressor. The tool can create geometry based on a few basic parameters and can be also be integrated with engineering sketch pad to generate solid blade models (Sharma et al., 2020). Following this, the quasi-3D optimization is performed using MISES and passed for further 3D CFD optimization in FINE/Turbo. The optimized 2D blade sections are stacked in T-Blade3 to generate 3D blades that may be meshed in Autogrid to generate a structured mesh with more than 5 levels of multigrid. The three-stage geometry is shown below in Figure 2. Table 1 displays the fillet and gap data, while Table 2 summarizes the grid data for steady state mesh. An alternative configuration of this three-stage design featuring shrouded stators was also explored and compared to this cantilevered configuration whose details can be found in (Ghimire and Turner, 2023).The first stage of this shrouded design has been experimentally tested at University of Notre Dame Turbomachinery Laboratory (NDTL) (Kang et al., 2024).

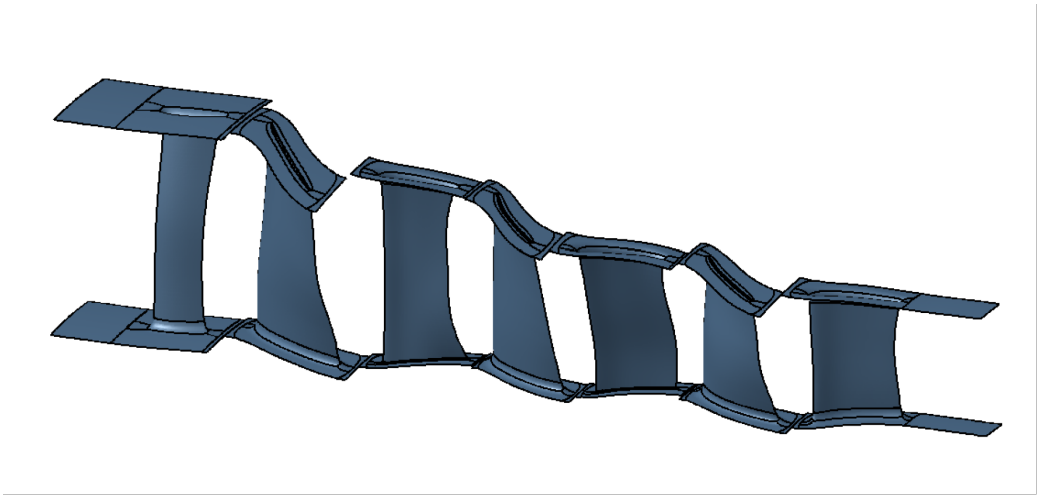

Figure 2 Three-stage 3D geometry

Row	LE Tip Radius (mm)	Hub Fillet(mm)	Tip Gap(mm)	Tip Fillet (mm)	Blade Count
IGV	134.79	1.6	-	1.6	43
R1	134.22	1.6	0.201	-	69
S1	131.56	1.6	-	1.6	114
R2	128.62	1.6	0.192	-	88
S2	126.24	1.6	-	1.6	112
R3	123.59	1.6	0.186	-	83
S3	122.09	1.6	-	1.6	101

Table 1. Gap and Fillet Data for Three-stage design

Row	Spanwise Points	No. of Grid Points
IGV	193	3.82 million
R1	289	9.9 million
S1	193	8.6 million
R2	305	11 million
S2	193	8 million
R3	305	10 million
S3	193	8 million
Total Grid Points		**60 million**
First Cell Width		1.2 X 10^{-7} m

Table 2. Grid Data

ii. Numerical Setup

MISES, an MIT developed code, is the selected CFD solver for Quasi-3D CFD. It is an Euler based CFD code that offers rapid performance analysis of cascade blade sections. Inviscid flow within the simulation is modeled using the Euler equations in MISES, the viscous flow is next solved with a 3D integral boundary layer. Transition is modeled using a modified Abu-Ghannam-Shaw transition model. Thermodynamic properties of sCO_2 are considered by MISES by adjusting the simulation specific heat ratio and Reynolds number.

The 3D CFD is performed with the suite of software by Cadence which includes FINE/Turbo as the flow solver. The fluid and thermodynamic properties of sCO_2 obtained from REFPROP (Huber et al., 2018) were formatted and imported to FINE/Turbo as condensable fluid. A grid sensitivity study was performed to validate the accuracy of various grid resolutions.

The fluid model was specified as thermodynamic tables for sCO_2 in the form of Saturation, PT, ER, HP, SP and HS tables. The flow was defined as steady with Turbulent Navier–Stokes flow model and the Spalart–Allmaras (SA) model was used for turbulence modeling. The SA model is dimensionally simple with one equation model which reduces the complexity of the problem and has been shown to give reliable results for boundary layers subjected to adverse pressure. Full Non-Matching Mixing Plane approach was used due to its capability to provide an exact conservation of the convective fluxes of mass, momentum, and energy through the interface and with less constraints on interface geometry to define rotor-stator interactions with zero order extrapolation which was deemed satisfactory. The boundary condition at inlet was defined by the total pressure profile generated from the estimation of the duct boundary layer at the University of Notre Dame's testing facility and the total temperature was set to be 371.15 K. A turbulent viscosity ratio of 50 was defined at the inlet. The mass-imposed boundary condition was used at the outlet with a design mass flow rate of 127 kg/s and initial pressure of 6.28 MPa. The rotation speed of 19,800 rpm was set for rotors.

Regarding the numerical scheme, the CFL number, which globally scales the time-step sizes used for the time-marching scheme of the flow solver was set to 2 to have the faster convergence but also to ensure the stability of the solution. The grid level 111 was selected for the computation. The grid sensitivity study was performed to validate the performance of grid level 111 (medium) mesh in comparison to the finer (000) mesh. No preconditioning was used. Cell centered control volume for spatial discretization and local time stepping technique for temporal discretization are used. The results for grid sensitivity study performed are shown below in Figure 3.

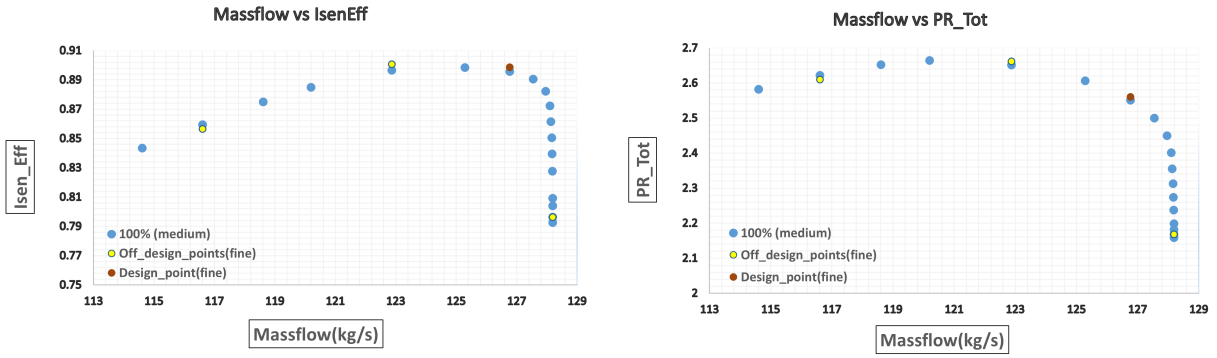

Figure 3. Grid sensitivity study. mass flow vs efficiency (left) and mass flow vs total pressure ratio (right)

The speed lines for the three-stage final design are shown in Figure 4. An efficiency of 89.85% and total pressure ratio of 2.61 at mass-flow rate of 125.86 kg/sec is predicted for the final design at the design point.

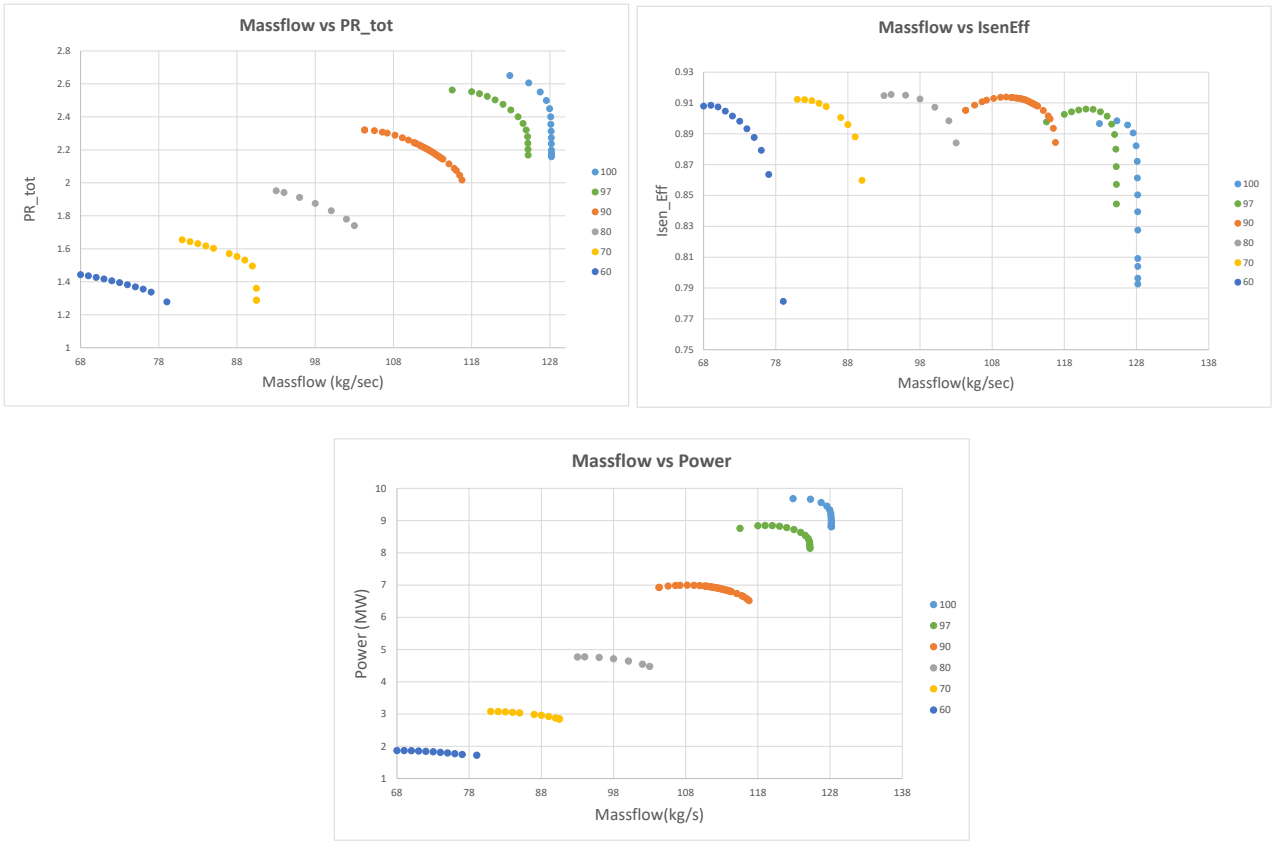

Figure 4. Speed lines for 3-stage design mass flow vs PR (left), mass flow vs efficiency(right) and mass flow vs Power(bottom)

IV. OPTIMIZATION

In broader context, optimization involves choosing the most favorable element based on specific criteria from a given set of options. At its core, an optimization problem aims to either maximize or minimize a real function by methodically selecting input values from a permissible set and evaluating the function's value. In our model, we employ the genetic driver within open-source optimization framework OpenMDAO (Gray et al., 2019) to optimize the geometry. The 3D optimization flow diagram is shown in Figure 5.

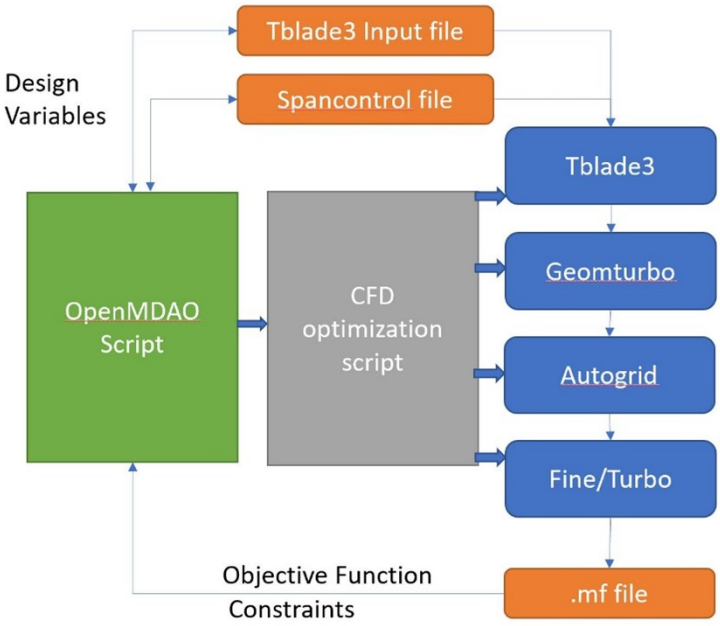

Figure 5. 3D optimization flow diagram

The combination of Latin Hypercube Sampling (LHS) and genetic algorithms (GAs) were used for optimization. Due to several advantages of GAs over other methods like being heuristic in nature, global search capability, parallelism, and particular robustness in noisy environments, they tend to be suitable for the approach like CFD based aerodynamic optimization. The approach is governed by careful selection of several parameters. The selection of population size depends upon how diverse the set of design variables are explored, and the number of generations determines the number of iterations/generations the GA will run. To allow for sufficient exploration along with having reasonable program execution time, 50 is selected as population size and number of generations. The number of bits is selected to be 8.

The crossover probability dictates how likely it is for a crossover to happen between two individuals. It is set to a value of 0.1. Mutation, on the other hand, is designed to change one or more gene values in a chromosome from their initial state. While some level of mutation is desired, excessive mutation can adversely impact the solution. Therefore, a parameter of 1% or 0.01 is chosen to regulate mutation in the process.

i. BUILDING STALL MARGIN

The major goal of the optimization was to arrive at the most efficient design geometry along with the improved stall margin. To facilitate this, the multi-objective functions chosen were to be the adiabatic efficiency at design point characterized by design exit Mach number along with the efficiency at the slightly reduced exit Mach number to improve the stall margin. Mach number was chosen as the exit boundary as it represents the exit corrected flow and allows us to navigate along operating line for different rotational speeds with different characteristics. The design variables selected for the aerodynamic optimization are the blade parameters such as blade metal angles (β^*_{in} and β^*_{out}), chord length, lean and sweep, These have been made possible due to the parametric nature of the inhouse built geometry tool modeler T-Blade3.

The optimization for the three-stage case has been performed at multipule fidelity levels. The details for the first stage design, optimization, and structural analysis has been presented in (Ha et al., 2022). Similarly, for the second and third stages, each span-wise section of the blade is first optimized using the same methodology. This quasi-3D optimization features a weighted objective function of design point and off-design point performance subject to turning to a constrained exit angle at the deisgn condition.

Gamma and Reynolds number are input into MISES. This leads to a strong 3D design for the initial geometry that may continue to high-fidelity optimization. The initial and quasi3D optimized R2 blade is shown in Figure 6. Similarly the results for S2 blade is shown in Figure 7. 3D optimization would improve factors that were not captured by the quasi-3D method, due to the 3D flow effects being ignored in MISES optimization.

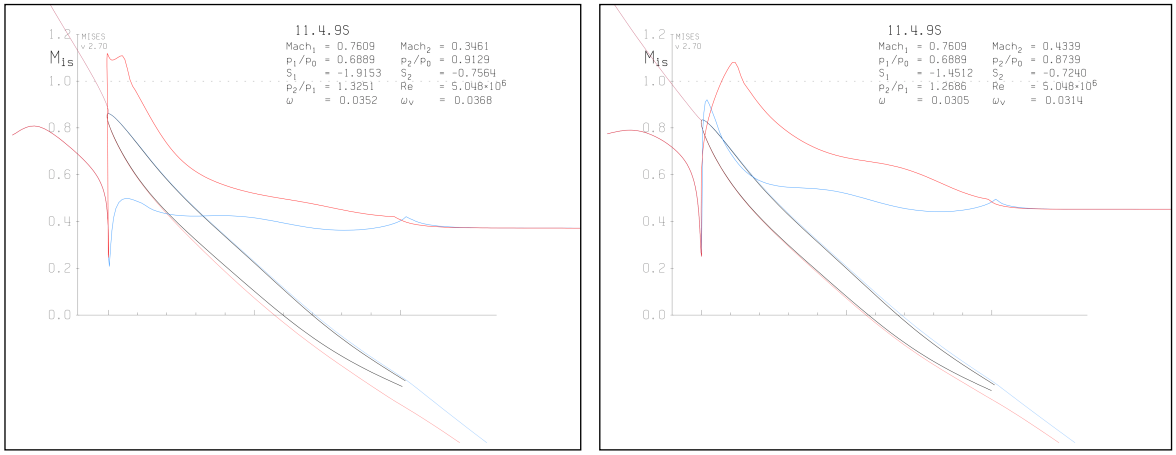

Figure 6 Isentropic Mach contours for 7-degree incidence at off-design (left) and design incidence(right) for R2 (MISES)

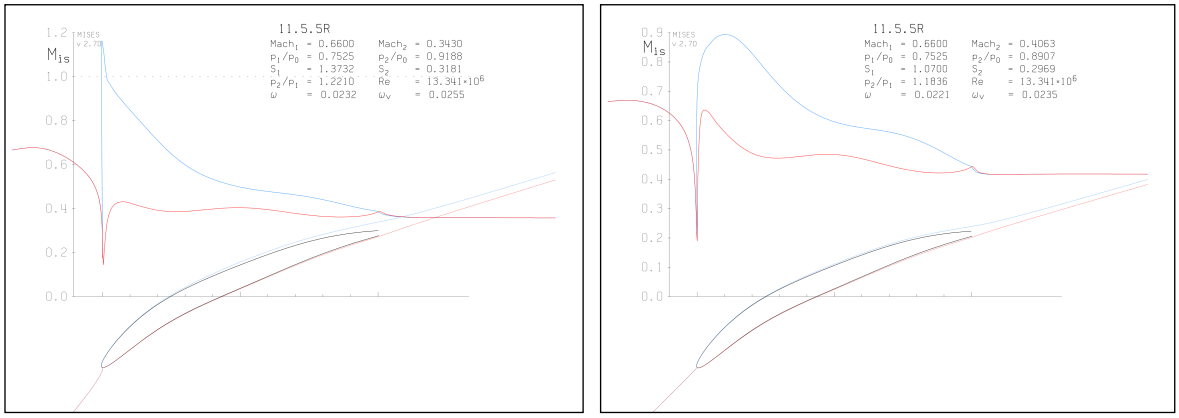

Figure 7 Isentropic Mach contours for 7-degree incidence at off-design (left) and design incidence(right) for S2 (MISES)

For 3D optimization of second and third stages, multi-objective optimization was performed for inlet and exit blade metal angles and chord multiplier. The approach was to optimize the hub (0 and 25% span), then the tip (75 and 100% span) and then the mid sections (25, 50, and 75% span). In addition to R2, S2 optimization would allow improvement at the hub so that S2 would take the small separation from R2 better. The inbeta* optimization pareto front at three mid-sections for S2 is shown in Figure 8. An improvement of 0.02% for design and 0.5% for near-stall efficiency was obtained for S2 which might not seem large but is significant when trying to improve an already quasi-3D optimized geometry.

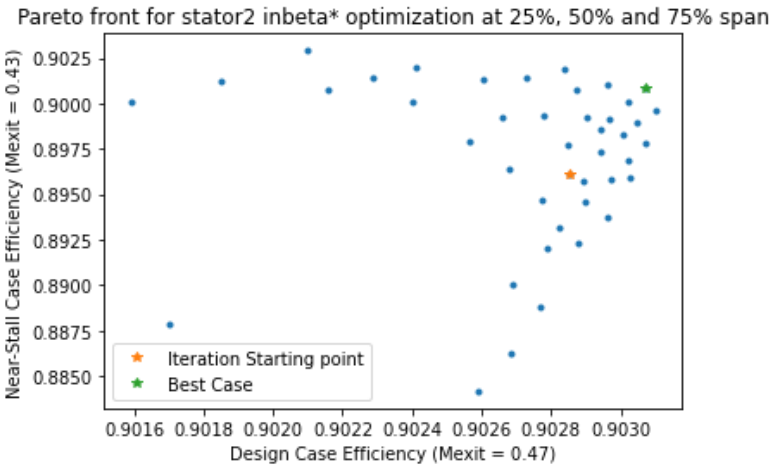

Figure 8 Blade inlet metal angle optimization at 25%,50% and 75% span for S2

V. STRUCTURAL ANALYSIS

Throughout the previously described optimization process, blade geometries were periodically analyzed using Ansys Mechanical to ensure structural integrity was maintained. At the design condition, a minimum safety factor constraint of 2 based on tensile yield of the material guided any necessary alterations to blade shapes. Once blade designs had been finalized, the to-be-manufactured shapes were determined by hot-to-cold transformation as described in (Holder et al., 2022).

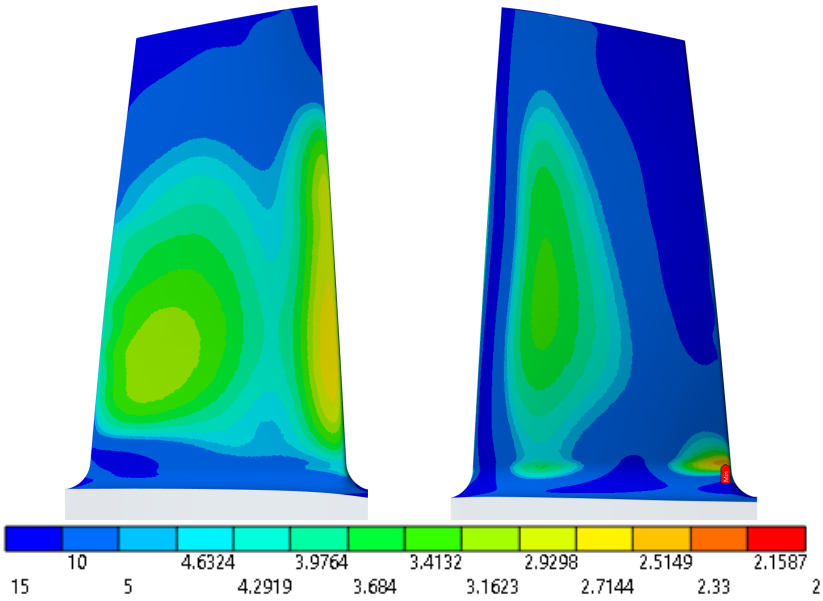

Figure 9 R2 safety factor contour on pressure side (left) and suction side (right).

The safety factor contour of R2 is shown in Figure 9. The stress concentration -- denoted by the red tag –

is on the suction side near the trailing edge just above the fillet where the safety factor reaches the minimum of 2.32. Figure 10 shows a similar concentration for R3, however, the pressure side midspan area is more highly stressed with a safety factor of 2.52.

Also, it is necessary, especially when designing an axial compressor to determine if a natural blade frequency is excited by a running frequency, its harmonics, or sub-harmonics. To determine this, Campbell diagrams for R2 and R3 were generated and are shown below in Figure 11. Both R2 and R3 show potential resonance points with adjacent stators but this is for higher order modes which require much more energy to excite. Lower modes were of most concern and both rotors have first modes greater than the four initial engine orders.

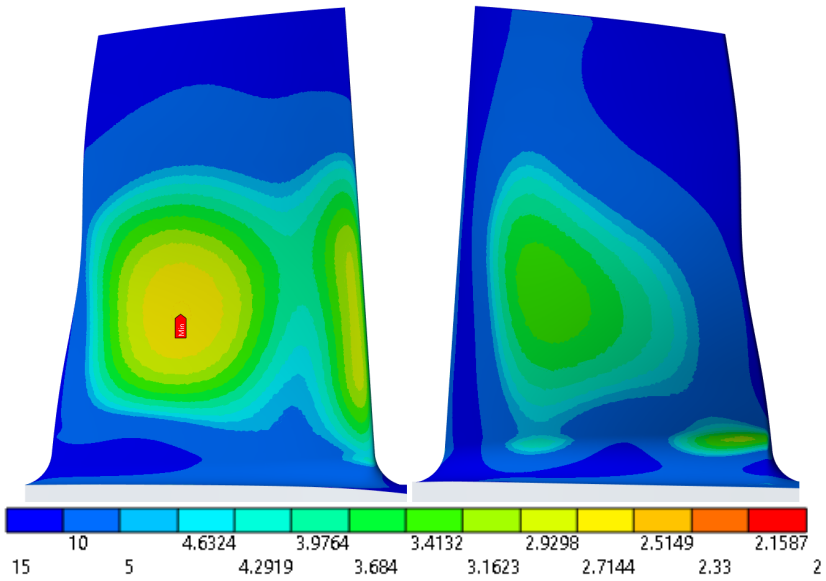

Figure 10 . R3 safety factor contour on pressure side (left) and suction side (right).

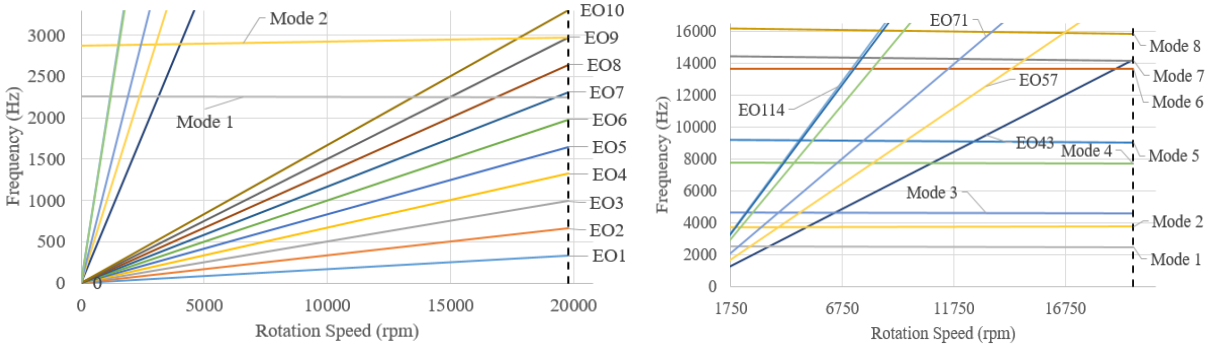

Figure 11 Campbell diagrams for R2 (left) and R3 (right)

CONCLUSION

A CFD based optimization methodology has been used to design the 3-stage axial sCO_2 compressor. The 3-stage compressor is the scaled down version of the larger nine-stage 100 MW design which was created to be manufactured and tested at University of Notre Dame Turbomachinery Laboratory. After the preliminary design including meanline and axisymmetric using the in-house built tools, the blade-to-blade sections were optimized using a parametric gradient based approach using MISES as the flow solver and included design point as well as off-design loss coefficient as the objective funciton. The resulting blade then became the baseline for 3D optimization. The consideration of design point and off-design point for both quasi-3D and full 3D optimization ensures range, or stall margin, as well as efficiency are part of the optimization process. The final design achieved the adiabatic efficiency of 89.85% and total pressure ratio of 2.61.

This work demonstrates the potential for optimization-based design methodology in real world applications. Notably, substantial enhancements in axial compressor performance were realized when permitting the optimizer to navigate the intricate blade design space influencing the complex flow physics within the transonic sCO_2 environment. Structural analyses were integral to the design process, revealing safety factors exceeding 2 for the hot shapes in static structural analysis. In the case of sCO_2, pressure loads contribute significantly to the blade stresses, particularly bending loads. Modal analyses, illustrated through the Campbell diagram, indicated the avoidance of resonance from the initial four system modes at any operating point.

REFERENCES

Brun, K., Friedman, P., Dennis, R., 2017. Fundamentals and Applications of Supercritical Carbon Dioxide (SCO2) Based Power Cycles. Woodhead Publishing.

Cline, S.J., Fessler, W., Liu, H.S., Lovell, R.C., Shaffer, S.J., n.d. High Pressure Compressor Component Performance Report (No. CR-168245). NASA.

David Hall, 2011. Performance Limits of Axial Turbomachine Stages. MASSACHUSETTS INSTITUTE OF TECHNOLOGY, Cambridge, Massachusetts.

Ghimire, S., Turner, M., 2023. Detailed Simulations of a Three-Stage Supercritical Carbon Dioxide Axial Compressor with a Focus on the Shrouded Stator Cavities Flow. Processes 11, 1358. https://doi.org/10.3390/pr11051358

Gray, J.S., Hwang, J.T., Martins, J.R.R.A., Moore, K.T., Naylor, B.A., 2019. OpenMDAO: an open-source framework for multidisciplinary design, analysis, and optimization. Struct. Multidiscip. Optim. 59, 1075–1104. https://doi.org/10.1007/s00158-019-02211-z

Ha, M., Holder, J., Ghimire, S., Ringheisen, A., Turner, M.G., 2022. Detailed Design and Optimization of the First Stage of an Axial Supercritical CO2 Compressor, in: Volume 10C: Turbomachinery — Design Methods and CFD Modeling for Turbomachinery; Ducts, Noise, and Component Interactions. Presented at the ASME Turbo Expo 2022: Turbomachinery Technical Conference and Exposition, American Society of Mechanical Engineers, Rotterdam, Netherlands, p. V10CT32A036. https://doi.org/10.1115/GT2022-82590

Holder, J.M., RingHeisen, A., Ha, M.J., Ghimire, S., Turner, M., 2022. Improved Automated Turbomachinery Hot-to-Cold Transformation With Cold-to-Hot Capabilities For Off-Design Analysis, in: AIAA SCITECH 2022 Forum. Presented at the AIAA SCITECH 2022 Forum, American Institute of Aeronautics and Astronautics, San Diego, CA & Virtual. https://doi.org/10.2514/6.2022-2436

Holloway, P.R., Knight, G.L., Koch, C.C., Shaffer, S.J., n.d. “Energy Efficient Engine High

Pressure Compressor Detail Design Report," (No. CR-165558). NASA.
Huber, M., Harvey, A., Lemmon, E., Hardin, G., Bell, I., McLinden, M., 2018. NIST Reference Fluid Thermodynamic and Transport Properties Database (REFPROP) Version 10 - SRD 23. https://doi.org/10.18434/T4/1502528
Kang, J., Vorobiev, A., Cameron, J., Morris, S., Wackerly, R., Sedlacko, K., Miller, J., Held, T., 2021. 10MW-Class sCO2 Compressor Test Facility at University of Notre Dame. Conf. Proc. Eur. SCO2 Conf. Eur. SCO2 Conf. Energy Syst. March 23-24 2021, 316. https://doi.org/10.17185/DUEPUBLICO/73975
Sharma, M., Dannenhoffer, J.F., Holder, J., Turner, M.G., 2020. Integration of an Open Source Blade Geometry Generator Using a Physics Based Parameterization With the Engineering Sketch Pad, in: Volume 2C: Turbomachinery. Presented at the ASME Turbo Expo 2020: Turbomachinery Technical Conference and Exposition, American Society of Mechanical Engineers, Virtual, Online, p. V02CT35A048. https://doi.org/10.1115/GT2020-15943
Sharma, M., Turner, M.G., 2021. Continuous Modified NACA Four-Digit Thickness Distribution for Turbomachinery Geometries. AIAA J. 59, 1501–1505. https://doi.org/10.2514/1.J060023
Turner, M.G., Merchant, A., Bruna, D., 2011. A Turbomachinery Design Tool for Teaching Design Concepts for Axial-Flow Fans, Compressors, and Turbines. J. Turbomach. 133, 031017. https://doi.org/10.1115/1.4001240
Wang, Y., Guenette, G., Hejzlar, P., Driscoll, M., 2004. Compressor Design for the Supercritical CO2 Brayton Cycle, in: 2nd International Energy Conversion Engineering Conference. Presented at the 2nd International Energy Conversion Engineering Conference, American Institute of Aeronautics and Astronautics, Providence, Rhode Island. https://doi.org/10.2514/6.2004-5722
Wells, K., Turner, M.G., 2021. Open Source Axial Compressor Mean-Line Design Tool for Supercritical Carbon Dioxide, in: Volume 10: Supercritical CO2. Presented at the ASME Turbo Expo 2021: Turbomachinery Technical Conference and Exposition, American Society of Mechanical Engineers, Virtual, Online, p. V010T30A024. https://doi.org/10.1115/GT2021-59961

ACKNOWLEDGEMENTS

The authors gratefully acknowledge the research project supported by the U.S. Department of Energy's Office of Energy Efficiency and Renewable Energy (EERE) under the Solar Energy Technologies Office Award Number DE-EE0008997. However, the views expressed herein do not necessarily represent the views of the U.S. Department of Energy or the United States Government.